Published in final edited form as:
J Neurosci. 2010 January 13; 30(2): 600–608. doi:10.1523/JNEUROSCI.4264-09.2010.

Conduction Block in PMP22 Deficiency

Yunhong Bai[1], **Xuebao Zhang**[2], **Istvan Katona**[1], **Mario Andre Saporta**[1], **Michael E. Shy**[1], **Heather A. O'Malley**[3], **Lori L. Isom**[3], **Ueli Suter**[4], and **Jun Li**[2,5]

[1]Department of Neurology, Wayne State University, Detroit, Michigan [2]Department of Neurology, Vanderbilt University, Nashville, Tennessee [3]Department of Pharmacology and Program in Cellular and Molecular Biology , University of Michigan, Ann Arbor, MI [4]Department of Biology, Institute of Cell Biology, ETH Zurich, Switzerland [5]Tennessee Valley Healthcare System-Nashville Campus, Tennessee, USA

Abstract

Patients with PMP22 deficiency present with focal sensory and motor deficits when peripheral nerves are stressed by mechanical force. It has been hypothesized that these focal deficits are due to mechanically induced conduction block (CB). To test this hypothesis, we induced 60-70% CB (defined by electrophysiological criteria) by nerve compression in an authentic mouse model of HNPP with an inactivation of one of the two *pmp22* alleles (*pmp22+/−*). Induction time for the CB was significantly shorter in *pmp22+/−* mice than that in *pmp22+/+* mice. This shortened induction was not found in the mice with deficiency of myelin protein zero (MPZ), a major structural protein of compact myelin. *Pmp22+/−* nerves showed intact tomacula with no segmental demyelination in both non-compressed and compressed conditions, normal molecular architecture, and normal concentration of voltage-gated sodium channels by H^3-saxitoxin binding assay. However, focal constrictions were observed in the axonal segments enclosed by tomacula, a pathological hallmark of HNPP. The constricted axons increase axial-resistance to action potential propagation, which should hasten the induction of CB in *pmp22* deficiency. Taken together, these results demonstrate that a function of Pmp22 is to protect the nerve from mechanical injury.

Keywords

PMP22; conduction block; paranode; tomacula; hereditary neuropathy with liability to pressure palsies (HNPP); Schwann cell; myelin; Charcot-Marie-Tooth disease; axonal constriction

INTRODUCTION

Peripheral myelin protein-22 (PMP22) is primarily expressed in the compact myelin of peripheral nerves and is encoded by the *PMP22* gene within the DNA segment of human chromosome 17p11.2 (Jetten and Suter, 2000). This gene is important clinically. Over-expression of *PMP22* causes Charcot Marie Tooth disease type 1A (CMT1A), the most common heritable neuropathy afflicting approximately 1:5000 people of all ethnic backgrounds (Nelis et al 1996). Alternatively, haploinsufficiency of *PMP22* results in a different disorder, hereditary neuropathy with liability to pressure palsies (HNPP) (Chance et al., 1993;Li J et al., 2007). Pathologically CMT1A is characterized by dys-/demyelination with frequent onion bulb formation (Robertson et al., 2002;Dyck and Lambert, 1968)

Corresponding author: Jun Li, MD, PhD, Department of Neurology, Vanderbilt University School of Medicine, 1161 21st Avenue South, Nashville, TN 37232. jun.li.2@vanderbilt.edu.

whereas HNPP is characterized by the presence of frequent focal myelin folds known as tomacula (Madrid R and Bradley G, 1975;Yoshikawa and Dyck, 1991).

HNPP is characterized by focal episodes of weakness and sensory loss (Marazzi et al., 1988;Li et al., 2004;Madrid R and Bradley G, 1975) These focal deficits are usually triggered by physical activities, including stretching, repetitive motions of affected limb or compression (Li et al., 2004), suggesting that there is nerve vulnerability to mechanical force in PMP22 deficiency. Whether this is the case remains to be demonstrated; an important issue that is not only clinically relevant but essential for understanding the biological function of PMP22 since HNPP is a “loss of function” model. These findings are not only clinically relevant but also reveal biological functions of PMP22, yet the underlying mechanisms are poorly understood.

PMP22 has been suggested to play a role in proliferation, differentiation and death of Schwann cells (Jetten and Suter, 2000;Sancho et al., 2001;Amici et al., 2007). These functions can be further evaluated in null models such as homozygous *Pmp22* deficient (*Pmp22* −/−) mice (Amici et al., 2007;Sancho et al., 2001). However, it is unlikely that any of these three functions play a role in HNPP, a heterozygous disorder, since *Pmp22* +/− mice, an authentic model of the human disease, have normal Schwann cell numbers and compact myelin (Adlkofer et al., 1997).

It has been hypothesized that the transient focal deficits in HNPP are caused by reversible conduction block (CB) (Lewis et al., 2000;Li et al., 2002;Li et al., 2004), a failed propagation of the action potential along myelinated nerve fibers (Cornblath et al., 1991;Kaji, 2003). To investigate this possibility and the role of PMP22 in nerve resistance to mechanical stress, we have created a CB model in *Pmp22* +/− mice by nerve compression. Our results demonstrated that CB can be mechanically induced in *Pmp22*+/− nerves more rapidly than in normal nerves.

METHODS

1. PMP22 deficient mice, genotyping and cross-breeding

The *pmp22+/−* mouse was generated by using homologous recombination technique to inactivate the *Pmp22* gene (Adlkofer et al., 1995). Peripheral nerves from this mouse showed typical pathological changes of HNPP, including tomacula (Adlkofer et al., 1995;Adlkofer et al., 1997). Due to cytomegalovirus infection, this mouse had to be re-derived embryonically to eliminate the viruses (assisted by Van Andel Rearch Institute, Grand Rapids, Michigan, USA). Re-derived mouse showed clinical phenotype and pathological changes identical to the mouse from original colony.

A breeding colony is maintained in Wayne State University animal facility. The Animal Investigational Committee in the institution has approved the use of animals for this study. For genotyping, DNA was isolated from clipped mouse tails, and subject to PCR analysis. Genotypes were determined as described in previous publications (Adlkofer et al., 1995;Adlkofer et al., 1997). For the control mice with heterozygous deletion of myelin protein zero (*MPZ*) and homozygous knockout of myelin-associate glycoprotein (*Mag*), procedures for breeding and genotyping have been described in previous publications (Shy et al., 1997;Yin et al., 1998).

To study axonal constriction, we have crossbred *pmp22+/−* mouse with *YFP* transgenic mouse (*YFPtg*+/+). *YFPtg* mouse was transferred from Dr. Derron Bishop’s laboratory and carries a transgene expressing yellow fluorescence protein (YFP) specifically in neurons

under the drive of *Thy-1* promotor (Bishop et al., 2004). This gives a clear and intense labeling of all axons.

2. *Nerve conduction study (NCS)*

Mice were anesthetized with Avertin (250mg/kg). Body temperature was allowed to equilibrate at room temperature. One pair of stimulating electrodes was positioned percutaneously at the sciatic notch. A second pair was inserted adjacent to the tibial nerve at the ankle. Compound muscle action potential (CMAP) was recorded from the intrinsic foot muscle using needle electrodes. CMAP amplitudes were measured from **baseline** to the peak of negative deflection. The ratio (P/D ratio) between CMAP amplitude from proximal and distal stimulation was calculated. This minimized the effect of changes in the absolute amplitude values due to variation in the electrode placement during different recordings in the same animals.

3. *Induction of CB by compression*

All mice in compression experiments were 2-3 month old. Anesthetized mice were placed on a styrofoam board. NCS was done as described above. CMAP was recorded prior to compression. CB was induced at tibial and sciatic nerves by two different techniques as described below.

CB at the tibial nerve—Mice were placed in prone position. The right leg rested on a metal plate with a width of 1 cm. Compression was delivered by a loop of nylon cord of 1 mm width with different weights attached (200 - 1000 grams). The cord ran cross the dorsal side of the leg 3 mm above the ankle to compress the tibial nerve (Figure 1A, B & C). Conduction velocities (CV) and P/D ratios were obtained every 15 minutes after the compression started. Toward the onset of CB, changes in conductions became accelerated. Thus, measurements were performed more frequently (every 5 minutes) until the ratio was reduced to 0.4 – 0.3 (60-70% CB). It has not been possible to make CB exactly at 60 or 70%, thus all CBs were targeted between 60-70%.

CB at the sciatic nerve—An incision was made around the sciatic notch to expose the sciatic nerve. The nerve was wrapped with 2 layers of gauze that was soaked with saline. Compression was applied on the surface of gauze with a $20g/mm^2$ vessel clamp (clamp width =1.5mm; Cat No = Tks-1-20g; Aros Surgical Instruments, Co). Conduction velocity and P/D ratios were collected as above.

4. *Semithin section and EM*

These techniques were described in our previous studies (Li et al., 2005;Zhang et al., 2008). In brief, mice were transcardially perfused with 4% paraformaldhyde and 3.5% glutaraldhyde. Sciatic or tibial nerves were dissected and post-fixed for 24 hours. Nerves were then osmicated for 1.5 hours, dehydrated, and embedded in Epon. Tissue blocks were sectioned with 1μm thickness and stained with methylene blue for light microscopic examination. The blocks were then trimmed and sectioned into ultrathin sections for EM examination (Zeiss EM 900).

For osmicated teased nerve fiber studies, nerves were dissected and fixed as described above, followed by dehydration and osmication in 1% osmium tetroxide before embedding in Epon. The nerve bundles were teased in fluid Epon under the dissection microscope using fine forceps. The glass slides with teased nerve fibers will be hardened in the 60°C oven, mounted with cover-slip, and examined under the light microscope.

5. *Teased nerve fiber immunohistochemistry (IHC)*

This technique has been described in our previous studies (Bai YH et al., 2006;Zhang et al., 2008). In brief, nerves were fixed in 4% paraformaldehyde for 30 minutes – 16 hours (depending on which primary antibodies to be used). Sciatic nerves were teased into individual fibers on glass-slides. The slides were dried overnight, reacted with primary antibodies, and stored at 4°C overnight, then incubated for 1.5 hours with secondary antibodies. The stained slides were examined under a Leica fluorescent or Nikon confocal microscope. All antibodies used are listed in Table 1.

6. *^{3}H-Saxitoxin binding assay (^{3}H-STX)*

Peripheral nerves, including bilateral sciatic, tibial, peroneal, roots and brachial plexus, were dissected from each mouse. Membrane protein extracts were prepared as previously described (Catterall et al., 1979). ^{3}H-STX binding was performed as described, using rat brain membranes as a positive control (Chen et al., 2002;Isom et al., 1995). Briefly, membrane extracts were washed in binding buffer (50 mM HEPES-Tris, pH 7.5, 130mM choline chloride, 5.4 mM KCL, 0.8 mM MgSO4, 5.5 mM dextrose). Membranes were then pelleted by centrifugation at 4°C and resuspended in ice-cold binding buffer. 200 μl of each sample was aliquoted into polypropylene tubes on ice (in triplicate), containing 25 μl of a 50 nM ^{3}H-STX stock (5 nM final concentration in the assay), plus 25 μl of 100 μM unlabeled tetrodotoxin stock (10 μM final) or binding buffer to assess non-specific binding. All samples were incubated on ice in a 4°C cold room for 1 hour. Binding was terminated by rapid vacuum filtration over Whatman GF/C filters that have been presoaked in wash buffer (163 mM choline chloride, 5 mM HEPES-Tris, pH 7.5, 1.8 mM CaCl, 0.8 mM $MgSO_4$) containing 1 mg/ml BSA, followed by 3 rapid washes with ice-cold wash buffer. ^{3}H-STX bound to the filters was assessed by scintillation counting. Specific binding is assessed by subtraction of non-specific binding in the presence of tetrodotoxin. Specific ^{3}H activity was normalized to protein concentration and finally expressed as fmol sodium channels per mg protein, based on the established 1:1 stoichiometry of STX binding to neuronal sodium channels. For each experiment, two samples were collected from 11-15 *pmp22+/+* mice and 11-15 *pmp22+/−* mice.

RESULTS

CB mechanically was induced more rapidly in Pmp22+/− nerves, but not in MPZ deficient nerves

To generate a model of CB in mice we performed a series of compressions on the tibial nerve using a nylon cord attached to different weights (200 – 1000g) (Figure 1A-1C). We identified an ideal weight of 400g that induces CB within 1.5 hours. The 400g weight was then used for the remaining experiments. Prior to compression, amplitudes of CMAP from proximal (P) and distal (D) stimulations were similar (Figure 1D). Within 4-5 minutes of compression, CMAP amplitude from proximal stimulation began to decrease and continued to drop if the compression was not removed. Once the P/D ratio reached 0.4 – 0.3, a 60-70% CB was diagnosed and the compression was removed (Figure 1D). There was a progressive prolongation of latencies with proximal stimulation prior to the CB while the distal motor latency remained unchanged, suggesting that there was focal slowing of conduction across the site of compression. Once 60-70% CB was achieved, the mice were returned to their cage. On waking from anesthesia (<1 hour), the mice dragged their compressed leg for approximately 12 hours. The compression system used in our experiments was chosen to deliver a mild force and minimize the possibility of axonal transection.

To examine susceptibility to compression in Pmp22 deficient nerves, we performed the compression experiments in 19 *Pmp22+/−* and 21 *Pmp22+/+* mice. The average time to

induce CB in the *Pmp22*+/− mice was 35±13 minutes, which was significantly shorter than with wild-type mice (55±38 minutes; $p<0.01$).

Tibial nerves are located on the medial side of the ankle in mice as well as humans. To determine whether different contact angles between nylon cord and the vertical line of the mouse leg were affecting our results, we performed another set of compression experiments in which we altered the angle by 15 degrees (arrow in Figure 1C). Similar results were observed. The mean duration for inducing CB between the *Pmp22*+/− mice (n=17) and wild-type (n=17) was 31.3±9.5 and 56.8±14.8 minutes (Figure 1G), which were again significantly different ($p<0.01$).

Tibial nerves are cushioned by skin and subcutaneous tissues which may vary from one mouse to another. In addition, the anatomical position of tibial nerves on the medial side of the ankle may also vary from mouse to mouse. To eliminate these potential factors, we surgically exposed sciatic nerves in the mice and compressed them directly using a vessel clamp (see technical details in Method section). Once again, the mean of duration for CB induction was shorter in *Pmp22*+/− mice than that in *Pmp22+/+* mice (17.0±4.4 vs 29.1±5.8 minutes; n=7 mice for each genotype; $p<0.001$).

To ensure that the shortened induction of CB is not due to the reduced CMAP amplitudes in *pmp22*+/− mice, we re-analyzed our data from both sets of experiments using nylon cord compression (32 *pmp22*+/− or 35 *pmp22*+/+ mice). Mice were separated into low and high CMAP groups. No significant difference between these groups was found in the onset of CB (supplementary Table 1; $p>0.05$).

To determine whether the shortened induction of CB is specific to the deficiency of Pmp22, we performed similar studies with heterozygous *mpz* knockout mice (*mpz*+/−). Like PMP22, MPZ is a major structural protein (>50% of all PNS myelin proteins) specific to compact myelin in the PNS (Shy et al., 2001). Deficiency of MPZ would be expected to negatively affect myelin stability. Indeed, homozygous deletion of *mpz* impairs myelin compaction (Martini et al., 1995), but abnormalities of myelin and axons occur even during embryonic stage and make the homozygotes unsuitable for control experiments. However, heterozygous null *mpz* (*mpz*+/−) mice do not develop significant electrophysiological and pathological abnormalities until the age of 6-12 months (Shy et al., 1997). Thus, prior to the age of 6 month old, they are an excellent animal model for controls. The induction time of CB on the compressed sciatic nerves was not significantly different between the *mpz*+/+ and *mpz*+/− mice (25.3±5.6 v.s. 25.3±6.9 minutes; n=6 mice for each genotypic group; $p>0.05$). In addition, teased nerve fiber studies on the sciatic nerves showed no segmental demyelination or tomacula in *mpz*+/− mice. Taken together, these data demonstrate that a function of Pmp22 is to protect the nerve from mechanical injury, which is not necessarily related to myelin stability.

CB mechanically induced more rapidly in mag+/– nerves

Next, we performed the nerve compression in *mag*–/− mice. We chose these animals because homozygous *mag* null mice also develop tomacula. Tomacula have been detected in nerves of these mice at one month of age and affect 50% of paranodes in 3-month-old *mag*–/− mice (Yin et al., 1998). This prevalence of tomacula is comparable to that in 6-month-old *pmp22*+/− mice. Heterozygous *mag* deficient mice (*mag*+/−), unlike heterozygous *pmp22*+/− animals, have no tomacula and no pathological phenotype (Yin et al., 1998). We therefore performed the compression experiments in *mag*–/− mice at 2 months of age. Surprisingly, teased nerve fiber examination showed no tomacula/axonal constrictions in *mag*–/− nerves. Nevertheless, CB was induced more rapidly in *mag*–/− mice than that in *mag*+/+ animals (9.0±2.5 v.s. 20.9±9.4 minutes; n=7 mice for each genotypic group; $p<0.01$). Since there

were no tomacula in these homozygous Mag deficient mice, this increased susceptibility to develop CB has to be caused by a different mechanism(s) than in the *pmp22*+/− mice. These findings suggest that vulnerability to mechanically induced CB in the peripheral nerves is not specific to Pmp22 deficiency, although the mechanisms for the CB may differ for different molecules.

Recovery of CB delayed in Pmp22 deficient nerves

NCS were repeated 3 or 5 days after the induction of CB in the first compression model, in which a nylon cord, attached to a weight, compressed the tibial nerve. CB completely recovered in 3 out of 5 wild-type mice by the 3rd day after compression and in 6 of the 7 wild-type mice by the 5th day (7th with a partial recovery) (Table 2 and Figure 1D). In contrast, CB showed no complete recovery in any of eleven *Pmp22*+/− mice at day 3 or day 5, and partial recovery in only half of the mice by day 5 (Table 2 and Figure 1E). These findings suggest that deficiency of Pmp22 results in slowed recovery from CB in the PNS.

To evaluate the pathological changes in the compressed nerves, we next obtained semithin sections at transverse 2-3mm distal to the compression site at both day 3 and 5 post compression. Axons with some signs of acute Wallerian degeneration were found in four of eleven *pmp22*+/− mice (n=12), but not in any of the wild-type mice (n=12). However, only two of twelve *pmp22*+/− mice had severe acute axonal degeneration, as defined by over two third of myelinated nerve fibers showing swelling and collapsed myelin (Figure 2).

We have also evaluated the recovery over multiple time points, using the 2nd compression model in which the sciatic nerve was compressed by a vessel clamp. The compressed nerves were harvested at day 0 (immediately after the compression), and at days 5, 7, 14, 21 and 30 (n=3 mice for each time point). The reduced CMAP amplitudes induced by the proximal stimulations were completely recovered by day 7 in the wild-type mice (distal CMAP = 6.9±2.6mV v.s. proximal CMAP = 6.4±2.5mV; $p>0.05$), but the recovery was delayed until day 14 in *pmp22*+/− mice (At day 7, distal CMAP = 2.4±0.6mV v.s. proximal CMAP = 1.9±0.5mV; At day 14, 2.7±0.5 v.s. 2.6±0.4).

To determine whether axonal size of mutant or wild type axons recovered differently following compression we evaluated axons at various time points after inducing CB. The nerves in both *pmp22+/+* and *pmp22+/−* mice appeared stretched with smaller diameters, losing their normal undulated, “wave-like” appearance under light microscopy (Figure 3). This undulated pattern and smaller diameters partially recovered at day 21, and returned to their normal state by day 30 post compression in both *pmp22+/+* and *pmp22*+/− nerves (supplementary Figure 1). Thus, persistent diffusely smaller diameters of axons could not explain the prolonged recovery from CB in the mutant animals.

Morphological examination at each time point demonstrated no or, at most, minimal damage in occasional axons in the compressed nerves of wild type mice (Figure 2 and supplementary Figure 1). However, axonal damages were found in all compressed sciatic nerves of *pmp22*+/− mice, but only limited to a small portion of nerve fibers (supplementary Figure 1). These degenerating axons were gradually diminishing during the recovery and were rarely detectable by day 30. In addition, on semithin sections, the prevalence of tomacula in the post-compressed nerves appeared similar to that in the nerves from the non-compressed side.

These results suggest that axonal injury was not contributing to CB in wild-type and played a minor role in Pmp22 deficient mice. However, the fact that a small portion of axons in Pmp22 deficient animals had some evidence of axonal damages suggested that Pmp22

insufficiency may make axons more susceptible to injury, which may contribute to the delayed recovery.

Compression does not cause axonal invagination, tomacula damage or segmental demyelination in pmp22+/− nerves

Nodal invagination has been considered to be the basis of mechanically induced CB in a series of elegant studies by Gilliatt and his colleagues (Ochoa, 1972;Ochoa et al., 1971;Rudge et al., 1974;Gilliatt et al., 1974;Ochoa et al., 1972). In these studies, either a tourniquet or a nylon cord with an attached weight was applied to baboon's limb, and reversible CB was induced without significant axonal damage. The results suggested that the early phase of CB was caused by displacement of the nodes at the edge of compression, so that the nodes invaginated into the adjacent paranodal area. In addition, paranodal myelin swelling and rupture were also noticed. However, in our osmicated teased nerve fibers, these changes in nodes/paranodes were not found unless we utilized a much stronger vessel clamp ($60g/mm^2$) to induce CB. Otherwise CB developed in the absence of nodal invagination in our model when milder compression was used.

Tomacula have been considered to be an unstable pathological structure that degenerates as animals age (Adlkofer et al., 1997). We hypothesized that Pmp22 deficient myelin may also be unstable and could break down during compression, causing CB. To address this issue, we examined the compressed sciatic nerves from our second compression model, CB induced by clamping exposed sciatic nerve. In this model the compressed nerve segment was wider and much easier to be identified. Despite of the fragility of the compressed nerves, we were still able to perform osmicated teased nerve fiber studies in three *pmp22*+/− and three *pmp22*+/+ mice. None of the >100 randomly selected myelinated nerve fibers from either *pmp22*+/− or *pmp22*+/+ mice showed disruption of myelin. All tomacula examined were intact. Thus, stability of tomacula and myelin did not explain predisposition to CB in our *Pmp22* +/− mice.

Molecular architecture and septate junctions of myelinated nerve fibers were normal in pmp22+/− mice

We next hypothesized that alterations of the molecular organization of *pmp22*+/− nerves might be responsible for the predisposition to develop CB, since these alterations are known to affect action potential propagation. Along these lines, recent investigations of myelinated axons and their nodes of Ranvier have demonstrated a surprising structural complexity, but very organized architecture, which is thought to be critical for the physiological functions of myelinated nerves (Scherer and Arroyo, 2002;Devaux and Scherer, 2005). To evaluate this architecture in our animals we performed teased nerve fiber IHC on non-compressed sciatic nerves from both *pmp22*+/− and *pmp22*+/+ mice. Proteins specific to each domain of myelinated nerve fibers, including node, paranode, juxtaparanode and internode, appeared well expressed and organized identically in mutant and wild type mice. These included Na_v in the nodes of Ranvier, Caspr and MAG in the paranodes, Kv1.2 in juxtaparanode and myelin basic protein (MBP) in internode (Figure 3). Therefore, alterations in the localization of these molecules could not explain the predisposition to develop CB in *Pmp22 +/−* mice.

We next investigated septate junctions, the structures that connect paranodal loops of myelinating Schwann cell membrane onto the paranodal axolemma. Thus, they seal the inner mesaxon space and separate the juxtaparanodes from nodes. Disrupting septate junctions would allow outward current from juxtaparanodal potassium channels to counteract the inward current from nodal Na_v, thereby raise the threshold of action potential production and decrease the safety factor for action potential propagation, resulting in CB (Lafontaine et al., 1982;Boyle et al., 2001). However, septate junctions in the paranodes

with tomacula appeared normal under EM, in longitudinal ultra-thin sections of non-compressed sciatic nerves (arrowheads in Figure 3F).

Although we had demonstrated a normal molecular architecture in non-compressed Pmp22 deficient nerves we recognize that Pmp22 deficiency may predispose changes in the molecular architecture during compression. We dissected sciatic nerves from mutant and wild type mice after CB was reached. IHC was performed with antibodies against Kv1.2 and Caspr. As with non-compressed nerves, no change of expression pattern of these proteins was found in the compressed sciatic nerves from either *pmp22*+/− or *pmp22*+/+ mice. However, axons appeared to have smaller diameters in the compressed nerves (Figure 3G, H and supplementary Figure 1).

Concentration of voltage-gated sodium channels (Na_v) was normal in pmp22+/− mice

Although the localization of Na_v appeared normal, we recognized that a decrease of Na_v concentration may also predispose CB by reducing the safety factor for action potential production (Kearney et al., 2002). We therefore performed a ^{3}H-STX binding assay to determine Na_v concentration in non-compressed peripheral nerves. Due to the overall low concentration of Na_v in the peripheral nerves (Lombet et al., 1985), we had to collect nerves from 11-15 mice of each genotype and pooled membrane proteins together for each experiment. Three experiments were done. The mean of Na_v concentration was 537±153 fmol/mg in *pmp22*+/+ mice and 603±132 fmol/mg in *pmp22*+/− mice; these differences were not significant ($P>0.05$). Thus the total quantity of Na_v could not explain the predisposition to CB in the mutant mice.

Axons encased by tomacula were constricted, a potential mechanism for shortened induction-time of CB in PMP22 insufficiency

Because there was no evidence of any myelin or molecular architecture change to explain the predisposition to CB in the preceding experiments, we next examined potential differences of axons between mutant and wild-type animals. We crossbred *pmp22*+/− mice with *YFPtg*+/+ mice. Axons in all offspring were labeled by YFP, so that axonal structures can be visualized with great clarity.

We found focal constrictions in the axonal segments enclosed by tomacula in non-compressed *pmp22*+/− myelinated nerve fibers (Figure 4B, C and F). We defined tomaculae as a focal enlargement of myelin by 1/3 of internodal diameter of the myelinated fiber. Axonal constriction was defined as segments with diameters reduced by 1/3 of the internodal axonal diameter. Axonal diameters decrease naturally in the nodal and paranodal regions of a normal myelinated nerve fiber (Figure 4A). Tomacula caused the axonal constriction to extend well beyond the paranodes. In some cases tomacula caused a greater reduction in axonal caliber than seen at nodes and paranodes (Figure 4B and C). To quantify this observation we randomly selected 20 paranodes with tomacula/axonal constrictions from 5 *pmp22*+/− mice and 20 paranodes without tomacula from 5 wild-type mice. Lengths of constricted axonal segments were measured in each paranode. The mean length of the constricted segments was 19.4±4.9 μm for paranodes with tomacula/constrictions and 4.2±0.2 μm for paranodes without tomacula ($p<0.0001$; Figure 4G).

The prevalence of tomacula and axonal constrictions was manually assessed in 50 randomly selected nodes from each 6-month-old *pmp22*+/− or *pmp22*+/+ mouse (n=5 mice for each genotype; Table 3). For most selected fibers, only one node in each myelinated fiber was evaluated. Regions with Schwann cell nucleus were avoided since there is a natural reduction of axonal diameter around the nucleus. Nearly half of the myelinated nerve fibers (48.4±12.3%) contained tomacula in 6-month-old *pmp22*+/− mice. Tomacula were mainly

found in the paranodal regions of *large* myelinated fibers (> 5 μm) although they occasionally occurred in the internodes. Because only one node was examined in each selected myelinated fiber, the actual prevalence of tomacula may even have been higher. 15.9±4.8% of all evaluated axons developed the focal constrictions. These constrictions were always within tomacula. Interestingly, a few axons in the tomacula (4.0±2.5%) were enlarged by at least 1/3 of internodal axonal diameter (Figure 4D). These enlargements presumably reflected axons that extended into myelin folds (Figure 4E and supplementary Figure 2B and C). Other axonal deformities within tomacula were also noticed (supplementary Figure 2). Overall, these pathological changes (tomacula, axonal constriction and enlargements) were present but slightly less (12% of evaluated axons) in 3-month-old *pmp22*+/− mice (Table 4).

We could not determine whether focal constrictions of mutant nerves under tomacula changed following compression by teased nerve fiber immunohistochemistry. The compressed nerves in all mice were fragile during mechanical manipulations such that any attempt at teasing nerve fibers introduced unacceptable artifact in the focally constricted region. As described above, we were able to perform osmicated teased nerve fiber study. However, the dark myelin prevents a clear visualization into the constricted regions of axons under the tomacula.

DISCUSSION

Our results demonstrate that mechanically induced CB occurs more rapidly and lasts longer in Pmp22 deficient nerves than in wild-type nerves. This finding was replicated in three sets of experiments by two different compression techniques. These findings confirm a hypothesis that has long been held concerning HNPP; namely that 50% of the normal PMP22 levels are inadequate to fully protect myelinated nerve fibers from compressive injury. Therefore one biological function of PMP22 must be protection from nerve injury.

The ease to develop CB cannot be explained simply because of reduced CMAP amplitudes in the mutant nerves (Figure 1E). CB was determined by using P/D ratio, not the absolute value of CMAP amplitudes. Moreover, when induction time of CB was compared between two groups of mice with low and high CMAP, no significant difference was found (supplementary Table 1). Therefore, we believe that CB is directly related to Pmp22 deficiency.

We have identified focal axonal constrictions within tomacula as a novel potential cause of increased susceptibility to CB in Pmp22 deficient mice. Axonal constrictions were identified only within segments enclosed by tomacula and were triple/quadruple the length of constricted segments normally found in nodes/paranodes. Reduced axonal diameter rapidly raises axial-resistance to action potential propagation since axial electric resistance of axons is inversely proportion to the square of axonal diameter (Hartline and Colman, 2007). Once the resistance increases to a critical level, CB occurs. We hypothesize that these multiple constricted axons within tomacula predispose the axons to CB. Furthermore, when the nerve is compressed, this causes even further stretching and thinning of axons (Figure 3G and supplementary Figure 1A). We postulate that this is the basis for the predisposition to CB observed in HNPP. Supporting our findings, reduced axonal diameters within tomacula have been identified in EM sections of sural nerve biopsies from patients with HNPP, although these findings were not quantified (Madrid R and Bradley G, 1975).

A potential concern for our hypothesis is whether the quantity of axonal constrictions we observed would be sufficient to predispose CB. Internodal length in mouse myelinated nerve fibers is 561±136μm (Perrot et al., 2007). A vessel clamp with a width of 1.5mm (1500μm)

covers 2-3 nodes. When one node per myelinated nerve fiber was examined in 3-month-old *Pmp22*+/− mice, 12% fibers showed focal axonal constrictions (Table 4). Thus, up to 36% of fibers, and most of the largest diameter fibers, have constrictions in nerve segments that are covered by the vessel clamp, which also means that 36% of fibers under the compression of a 1.5mm width clamp are predisposed to CB. More importantly, it is the large myelinated fibers that are responsible for the major portion of CMAP, which is reduced in CB. For instance, with stronger and longer compression to achieve 60-100% CB in previous studies, pathological changes were still observed mainly in large myelinated fibers (Ochoa et al., 1972), and small fibers were spared (Ochoa et al., 1972;Fowler TJ and Ochoa J, 1975). In fact, early occurrence of slowing across the compression site in our experiments and previous compression studies (Rudge et al., 1974) also indicated that the large myelinated fibers were preferentially affected since conduction velocity measures the conduction of largest myelinated fibers (Gasser HS and Grundfest H, 1939). Finally, other pathological alterations in *pmp22*+/− nerves, such as the enlargements of paranodal axons in the tomacula (Figure 4D and E), may also contribute to the rapid induction of CB. These convoluted axolemma may increase the total areas of paranodal axolemma and raise the capacitance, leading to a reduction of safety factor for action potential propagation (Joyner et al., 1980).

Our data do not claim that axonal constrictions in tomacula are the only cause for the CB. For example, wild type mice also developed a decline in CMAP amplitudes after 5 minutes of compression and CB within 30 minutes. It simply occurs more rapidly in the mutant mice for a given level of compression. We do not know what other factors cause CB in wild type animals. However the classical studies of Gilliatt and colleagues implicating nodal invagination cannot explain CB in our models since even wild type mice did not demonstrate nodal invagination associated with their block unless stronger compression was applied.

How tomacula and axonal constrictions are formed remains a mystery. Tomaculae are not unique to PMP22 insufficiency. They have been found in other neuropathies and animal models, including anti-MAG neuropathy, CMT1B, chronic inflammatory demyelinating neuropathy, Tangier's disease, as well as several animal models of peripheral nerve disorders (Sander et al., 2000;Cai et al., 2006;Cai et al., 2002). It has been hypothesized that tomacula result from excessive myelin folding collapsed on constricted axons in MAG knockout mice (Yin et al., 1998). However, these findings have been challenged after focal hypermyelination was found in *mag*−/− mice at young age when axonal diameters were still normal (Cai et al., 2002). Thus, these findings suggest that tomaculae are formed first and subsequently induce focal axonal constrictions by unknown mechanisms in MAG deficiency, such as abnormal Schwann cell-axon interaction. Whether this is also the case in PMP22 deficiency remains to be clarified. Whether there is an abnormal signaling through MAG in PMP22 deficiency is also unknown. Nevertheless, our data suggest that normal dosage of PMP22 is required to prevent formation of axonal constriction, which may be the mechanism of the protection it provides from nerve injury.

Finally, we have found axonal damage in a small portion of *pmp22*+/− nerves that were compressed. These alterations disrupted axons between the proximal and distal stimulation sites and produce what might initially appear as CB (pseudo-CB). However, evidence of Wallerian degeneration was not seen in the vast majority of axons and is not a viable explanation for CB for our results. We do not know what other factors contributed to the delayed recovery from CB in the mutant mice. Our results did not show a delayed recovery in mutant mice from nerve stretching or an increased number of tomacula in the post-compressed nerve fibers. It is still possible that a delayed recovery of focally constricted axons, under tomacula, is a contributing factor.

Acute axonal damage occurred only rarely in *pmp22+/−* mice, it does have important clinical significance. In one case report, a 20-year-old woman with HNPP developed massive axonal degeneration in her arms after strenuous physical activities, including running with a 34kg backpack and performing 150 push-ups a day (Horowitz et al., 2004). We have also identified a similar case. This 48-year-old man with HNPP developed arm weakness after heavy weight lifting. Needle EMG showed significant denervation in his arms, demonstrating that he had undergone acute Wallerian degeneration. Taken together, mechanical challenges during long or extraneous physical activities may be safe for normal people, but could be dangerous to patients with HNPP.

Supplementary Material

Refer to Web version on PubMed Central for supplementary material.

Acknowledgments

Authors thank Ms. Yanmei Yuan for her technical assistance. This research is supported by grants from the NINDS (K08 NS048204 to J.L.), MDA (MDA 4029 to J.L.), Veteran Administration (B6243R to J.L.), the Swiss National Science Foundation and the NCCR Neural Plasticity and Repair (to US), National Multiple Sclerosis Society (RG2882 and RG3771A4/3 to LLI), the University of Michigan Training Program in Cellular and Molecular Biology (NIH GM007315-31 to HOM) and University of Michigan Rackham Predoctoral Fellowship to HOM.

Reference List

1. Adlkofer K, Frei R, Neuberg DH, Zielasek J, Toyka KV, Suter U. Heterozygous peripheral myelin protein 22-deficient mice are affected by a progressive demyelinating tomaculous neuropathy. J Neurosci. 1997; 17:4662–4671. [PubMed: 9169527]
2. Adlkofer K, Martini R, Aguzzi A, Zielasek J, Toyka KV, Suter U. Hypermyelination and demyelinating peripheral neuropathy in Pmp22-deficient mice. Nat Genet. 1995; 11:274–280. [PubMed: 7581450]
3. Amici SA, Dunn WA Jr. Notterpek L. Developmental abnormalities in the nerves of peripheral myelin protein 22-deficient mice. J Neurosci Res. 2007; 85:238–249. [PubMed: 17131416]
4. Bai YH, Ianokova E, Pu Q, Ghandour K, Levinson R, Martin JJ, Ceuterick-de Groote C, Mazanec R, Seeman P, Shy ME, Li J. R69C Mutation in P0 Gene Alters Myelination and Ion Channel Subtypes. Archives of Neurology. 2006; 63:1787–1794. [PubMed: 17172621]
5. Bishop DL, Misgeld T, Walsh MK, Gan WB, Lichtman JW. Axon branch removal at developing synapses by axosome shedding. Neuron. 2004; 44:651–661. [PubMed: 15541313]
6. Boyle ME, Berglund EO, Murai KK, Weber L, Peles E, Ranscht B. Contactin orchestrates assembly of the septate-like junctions at the paranode in myelinated peripheral nerve. Neuron. 2001; 30:385–397. [PubMed: 11395001]
7. Cai Z, Blumbergs PC, Cash K, Rice PJ, Manavis J, Swift J, Ghabriel MN, Thompson PD. Paranodal pathology in Tangier disease with remitting-relapsing multifocal neuropathy. J Clin Neurosci. 2006; 13:492–497. [PubMed: 16678735]
8. Cai Z, Sutton-Smith P, Swift J, Cash K, Finnie J, Turnley A, Thompson PD, Blumbergs PC. Tomacula in MAG-deficient mice. J Peripher Nerv Syst. 2002; 7:181–189. [PubMed: 12365566]
9. Catterall WA, Morrow CS, Hartshorne RP. Neurotoxin binding to receptor sites associated with voltage-sensitive sodium channels in intact, lysed, and detergent-solubilized brain membranes. J Biol Chem. 1979; 254:11379–11387. [PubMed: 500648]
10. Chance PF, Alderson MK, Leppig KA, Lensch MW, Matsunami N, Smith B, Swanson PD, Odelberg SJ, Disteche CM, Bird TD. DNA deletion associated with hereditary neuropathy with liability to pressure palsies. Cell. 1993; 72:143–151. [PubMed: 8422677]
11. Chen C, Bharucha V, Chen Y, Westenbroek RE, Brown A, Malhotra JD, Jones D, Avery C, Gillespie PJ III, Kazen-Gillespie KA, Kazarinova-Noyes K, Shrager P, Saunders TL, Macdonald RL, Ransom BR, Scheuer T, Catterall WA, Isom LL. Reduced sodium channel density, altered

voltage dependence of inactivation, and increased susceptibility to seizures in mice lacking sodium channel beta 2-subunits. Proc Natl Acad Sci U S A. 2002; 99:17072–17077. [PubMed: 12481039]

12. Cornblath DR, Sumner AJ, Daube J, Gilliat RW, Brown WF, Parry GJ, Albers JW, Miller RG, Petajan J. Conduction block in clinical practice. Muscle Nerve. 1991; 14:869–871. [PubMed: 1922183]
13. Devaux JJ, Scherer SS. Altered ion channels in an animal model of Charcot-Marie-Tooth disease type IA. J Neurosci. 2005; 25:1470–1480. [PubMed: 15703401]
14. Dyck PJ, Lambert EH. Lower motor and primary sensory neuron diseases with peroneal muscular atrophy. I. Neurologic, genetic, and electrophysiologic findings in hereditary polyneuropathies. Arch Neurol. 1968; 18:603–618. [PubMed: 4297451]
15. Fowler TJ, Ochoa J. Unmyelinated fibers in normal and compressed peripheral nerves of the baboon: a quantitative electron microscopic Study. Neuropathology and Applied Neurobiology. 1975; 1:247–265.
16. Gasser HS, Grundfest H. Axon diameter in relation to the spike dimentions and conduction velocity in Mammalian A fibers. American Journal of Physiology. 1939; 127:393–414.
17. Gilliatt RW, McDonald WI, Rudge P. Proceeding: The site of conduction block in peripheral nerves compressed by a pneumatic tourniquet. J Physiol. 1974; 238:31P–32P.
18. Hartline DK, Colman DR. Rapid conduction and the evolution of giant axons and myelinated fibers. Curr Biol. 2007; 17:R29–R35. [PubMed: 17208176]
19. Hess A, Young JZ. The nodes of Ranvier. Proceedings of Royal Society, Series B. 1952; 140:301–320.
20. Horowitz SH, Spollen LE, Yu W. Hereditary neuropathy with liability to pressure palsy: fulminant development with axonal loss during military training. J Neurol Neurosurg Psychiatry. 2004; 75:1629–1631. [PubMed: 15489403]
21. Isom LL, Scheuer T, Brownstein AB, Ragsdale DS, Murphy BJ, Catterall WA. Functional co-expression of the beta 1 and type IIA alpha subunits of sodium channels in a mammalian cell line. J Biol Chem. 1995; 270:3306–3312. [PubMed: 7852416]
22. Jetten AM, Suter U. The peripheral myelin protein 22 and epithelial membrane protein family. Prog Nucleic Acid Res Mol Biol. 2000; 64:97–129. [PubMed: 10697408]
23. Joyner RW, Westerfield M, Moore JW. Effects of cellular geometry on current flow during a propagated action potential. Biophys J. 1980; 31:183–194. [PubMed: 7260286]
24. Kaji R. Physiology of conduction block in multifocal motor neuropathy and other demyelinating neuropathies. Muscle Nerve. 2003; 27:285–296. [PubMed: 12635114]
25. Kearney JA, Buchner DA, de Haan G, Adamska M, Levin SI, Furay AR, Albin RL, Jones JM, Montal M, Stevens MJ, Sprunger LK, Meisler MH. Molecular and pathological effects of a modifier gene on deficiency of the sodium channel Scn8a (Na(v)1.6). Hum Mol Genet. 2002; 11:2765–2775. [PubMed: 12374766]
26. Lafontaine S, Rasminsky M, Saida T, Sumner AJ. Conduction block in rat myelinated fibres following acute exposure to anti-galactocerebroside serum. J Physiol. 1982; 323:287–306. [PubMed: 7097575]
27. Lewis RA, Sumner AJ, Shy ME. Electrophysiological features of inherited demyelinating neuropathies: A reappraisal in the era of molecular diagnosis. Muscle Nerve. 2000; 23:1472–1487. [PubMed: 11003782]
28. Li J, Ghandour K, Radovanovic D, Shy RR, Krajewski KM, Shy ME, Nicholson GA. Stoichiometric alteration of PMP22 protein determines the phenotype of HNPP. Archives of Neurology. 2007; 64:974–978. [PubMed: 17620487]
29. Li J, Bai Y, Ghandour K, Qin P, Grandis M, Trostinskaia A, Ianakova E, Wu X, Schenone A, Vallat JM, Kupsky WJ, Hatfield J, Shy ME. Skin biopsies in myelin-related neuropathies: bringing molecular pathology to the bedside. Brain. 2005; 128:1168–1177. [PubMed: 15774502]
30. Li J, Krajewski K, Lewis RA, Shy ME. Loss-of-function phenotype of hereditary neuropathy with liability to pressure palsies. Muscle Nerve. 2004; 29:205–210. [PubMed: 14755484]
31. Li J, Krajewski K, Shy ME, Lewis RA. Hereditary neuropathy with liability to pressure palsy: the electrophysiology fits the name. Neurology. 2002; 58:1769–1773. [PubMed: 12084875]

32. Lombet A, Laduron P, Mourre C, Jacomet Y, Lazdunski M. Axonal transport of the voltage-dependent Na+ channel protein identified by its tetrodotoxin binding site in rat sciatic nerves. Brain Res. 1985; 345:153–158. [PubMed: 2415212]
33. Madrid R, Bradley G. The pathology of neuropathies with focal thickening of the myelin sheath (tomaculous neuropathy): studies on the formation of the abnormal myelin sheath. Journal of The Neurological Sciences. 1975; 25:415–448.
34. Marazzi R, Pareyson D, Scaioli V, Corbo M, Boiardi A, Chiodelli G, Sghirlanzoni A. Recurrent familial neuropathy due to liability to pressure palsies. Ital J Neurol Sci. 1988; 9:355–363. [PubMed: 3220711]
35. Martini R, Mohajeri MH, Kasper S, Giese KP, Schachner M. Mice doubly deficient in the genes for P0 and myelin basic protein show that both proteins contribute to the formation of the major dense line in peripheral nerve myelin. J Neurosci. 1995; 15:4488–4495. [PubMed: 7540676]
36. Ochoa J. Ultrathin longitudinal sections of single myelinated fibres for electron microscopy. J Neurol Sci. 1972; 17:103–106. [PubMed: 4626884]
37. Ochoa J, Danta G, Fowler TJ, Gilliatt RW. Nature of the nerve lesion caused by a pneumatic tourniquet. Nature. 1971; 233:265–266. [PubMed: 4999642]
38. Ochoa J, Fowler TJ, Gilliatt RW. Anatomical changes in peripheral nerves compressed by a pneumatic tourniquet. J Anat. 1972; 113:433–455. [PubMed: 4197303]
39. Perrot R, Lonchampt P, Peterson AC, Eyer J. Axonal neurofilaments control multiple fiber properties but do not influence structure or spacing of nodes of Ranvier. J Neurosci. 2007; 27:9573–9584. [PubMed: 17804618]
40. Robertson AM, Perea J, McGuigan A, King RH, Muddle JR, Gabreels-Festen AA, Thomas PK, Huxley C. Comparison of a new pmp22 transgenic mouse line with other mouse models and human patients with CMT1A. J Anat. 2002; 200:377–390. [PubMed: 12090404]
41. Rudge P, Ochoa J, Gilliatt RW. Acute peripheral nerve compression in the baboon. J Neurol Sci. 1974; 23:403–420. [PubMed: 4427124]
42. Sancho S, Young P, Suter U. Regulation of Schwann cell proliferation and apoptosis in PMP22-deficient mice and mouse models of Charcot-Marie-Tooth disease type 1A. Brain. 2001; 124:2177–2187. [PubMed: 11673320]
43. Sander S, Ouvrier RA, McLeod JG, Nicholson GA, Pollard JD. Clinical syndromes associated with tomacula or myelin swellings in sural nerve biopsies. J Neurol Neurosurg Psychiatry. 2000; 68:483–488. [PubMed: 10727485]
44. Scherer SS, Arroyo EJ. Recent progress on the molecular organization of myelinated axons. J Peripher Nerv Syst. 2002; 7:1–12. [PubMed: 11939347]
45. Shy ME, Arroyo E, Sladky J, Menichella D, Jiang H, Xu W, Kamholz J, Scherer SS. Heterozygous P0 knockout mice develop a peripheral neuropathy that resembles chronic inflammatory demyelinating polyneuropathy (CIDP). J Neuropathol Exp Neurol. 1997; 56:811–821. [PubMed: 9210878]
46. Shy ME, Balsamo J, Lilien J, Kamholz J. A molecular basis for hereditary motor and sensory neuropathy disorders. Curr Neurol Neurosci Rep. 2001; 1:77–88. [PubMed: 11898503]
47. Yin X, Crawford TO, Griffin JW, Tu P, Lee VM, Li C, Roder J, Trapp BD. Myelin-associated glycoprotein is a myelin signal that modulates the caliber of myelinated axons. J Neurosci. 1998; 18:1953–1962. [PubMed: 9482781]
48. Yoshikawa H, Dyck PJ. Uncompacted inner myelin lamellae in inherited tendency to pressure palsy. J Neuropathol Exp Neurol. 1991; 50:649–657. [PubMed: 1895146]
49. Zhang X, Chow CY, Sahenk Z, Shy ME, Meisler MH, Li J. Mutation of FIG4 causes a rapidly progressive, asymmetric neuronal degeneration. Brain. 2008

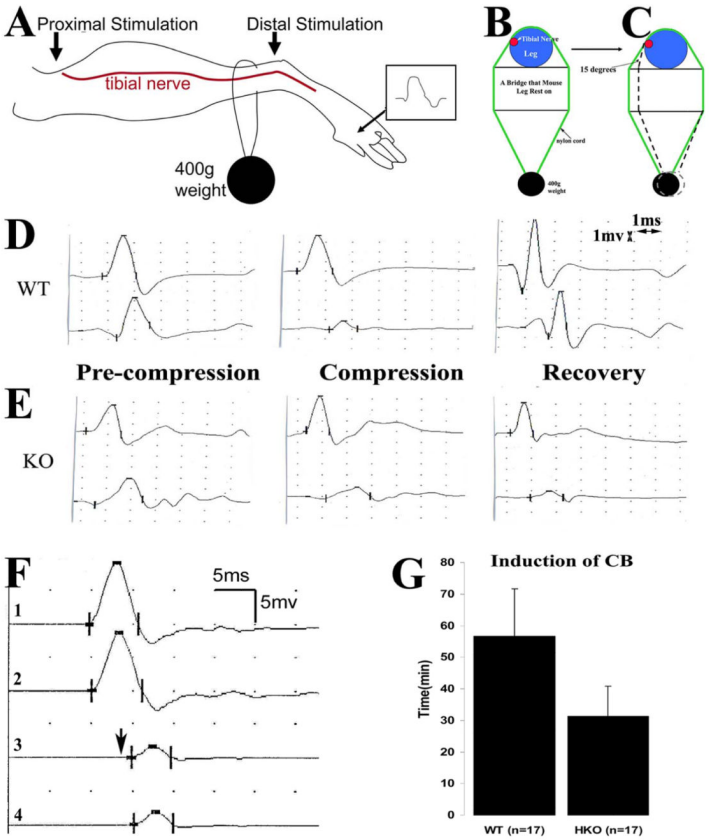

Figure 1. Experimental paradigm for nerve compression, and mechanically induced CB in mice

A. This diagram shows the placement of stimulation (arrows) and recording (marked by R) electrodes for NCS. B. Compression was delivered by a nylon cord loop attached a 400g weight. This diagram shows the cross-section at the site of nylon cord. The leg rests on a metal plate (marked as 'bridge') with a width of about 1 cm. Tibial nerves usually run on the medial side of the ankle (red dot). C. In the second set of experiments, the angle between the nylon cord and the vertical line of leg is reduced by 15 degrees by shortening the length of the bridge (arrow in C). D. An example of NCS from a compression experiment on a wild-type mouse is shown. In the D-left figure, similar amplitudes of CMAP were evoked by stimulations at the distal and proximal sites. After compression was applied, CMAP amplitude from the proximal stimulation was reduced >60% of the CMAP amplitude by the distal stimulation, called CB (D-middle figure). At this point, compression was removed. At the day 5 after the compression, CB recovered (D-right figure). E. The same experiment was performed on a *pmp22*+/− mouse. CB did not recover at day 5 following compression (E-right figure). Sensitivity = 1mV; Speed = 1ms. Notice that the onset of CMAP in mice may be obscured by an evolving positive-deflection. Thus, peaks of CMAP were often used to calculate the latency and conduction velocity. Nevertheless, this issue does not affect the measurement of CMAP amplitudes or any of our conclusions. F. An original trace recorded at the hypothenar muscle of *a patient* with HNPP: Stimulations on the ulnar nerve inched 1 cm/step across the elbow, a location subject to compression. A focal slowing (a long delay from trace 2 to 3 in contrast to a very short delay from 1 to 2 or from 3 to 4) across the elbow was identified within a 1cm segment of the nerve, demonstrating the very focal nature of the slowing. CB was conspicuous in this case. Arrow indicated the third response which had a >50% amplitude drop of motor response, and was associated with weakness in muscles innervated by the ulnar nerve. G. Induction time for CB was compared between

wild-type and *pmp22*+/− mice in the second set of experiments (see 1C) and was significantly shorter in *pmp22*+/− mice ($p<0.01$; **error bars = standard deviation**).

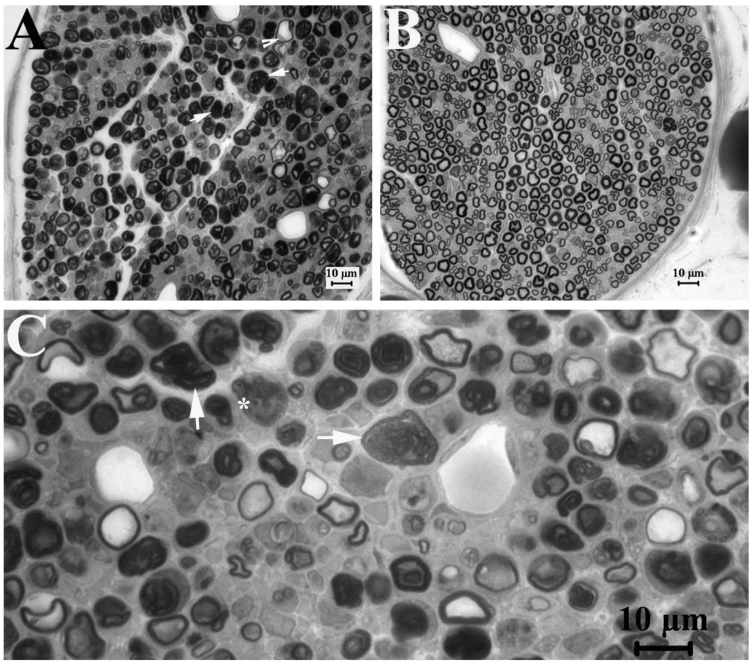

Figure 2. Axonal injuries in compressed PMP22-insufficient nerves

At post-compression day 3 and 5 we obtained semithin sections at transverse 2-3mm distal to the compression site, and examined them under light microscopy. Axons with signs of acute Wallerian degeneration, including extensively collapsed myelin (arrows in 2A and C with high magnification), degenerated axons (asterisk in 2C) and swelled nerve fibers (arrowhead in 2A), were found in four of eleven *pmp22*+/− mice (n=11), but not in wild-type mice (n=12; 2B). Two of these four *pmp22*+/− mice were severe (2A). These results suggest that Pmp22 insufficiency may make nerve susceptible to axonal injuries in a small portion of animals.

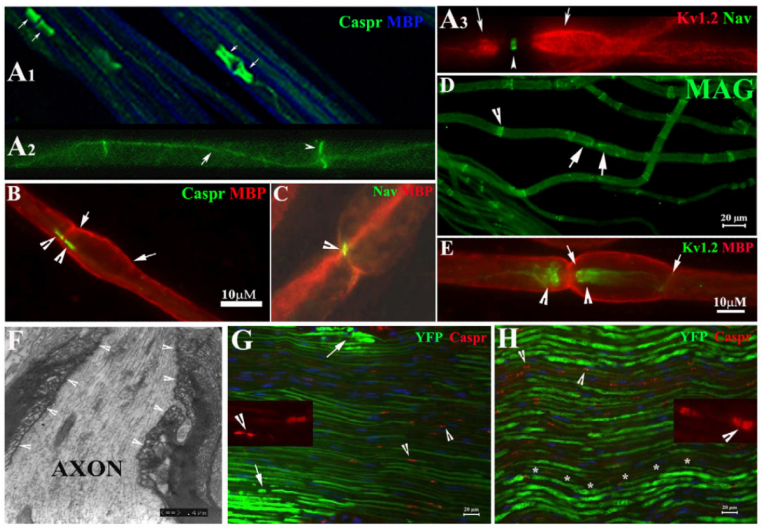

Figure 3. Molecular architecture and septate junctions in naïve and compressed nerves

A1-3. Wild-type mice at 2-3-month-old age were perfused. *Non-compressed* sciatic nerves were dissected and teased into individual nerve fibers. Slides were stained with antibodies against MBP (blue) and Caspr (green). The former revealed internodal myelin (blue in A1). Caspr stained paranodes (arrows) that flanked the node of Ranvier. Caspr was also expressed at the Schmidt-Lanterman incisures (arrowhead in A2) and along the inner mesaxon as it spirals around the axon (arrow in A3). Voltage-gated potassium channels (Kv1.2; red in A3) were found in the juxtaparanodes (arrows in A3). Na_v were concentrated in the node of Ranvier (arrowhead in A3) and appeared as a narrow band. B-E was from non-compressed *pmp22*+/− nerves. Na_v, Kv1.2, Caspr and MBP were all localized in their proper regions. In addition, MAG was also correctly localized in the paranodes (arrows in D) and incisures (arrowhead in D) similar to what was observed in the wild-type myelinated nerve fibers. Tomacula were mainly found in the paranodal regions (B and E) and almost always extended beyond the paranodes and into juxtaparanodes and internodes (between arrows in B and E). F. EM was performed on the longitudinal section of a non-compressed *pmp22*+/− sciatic nerve. Normal paranodal septate junctions (arrowhead array) were observed in the region with tomacula. G. *Compressed* sciatic nerves from the second compression model (surgically exposed and clamped sciatic nerve) and non-compressed sciatic nerves (H) were sectioned into 10μm thickness and stained with antibodies against Caspr. Localization of Caspr in the paranodes (**arrowheads in G and insets**, and in supplementary Figure 1) was normal in compressed nerves. So was Kv1.2. However, axons revealed by YFP had smaller diameters and appeared stretched (G). Supporting this notion, we observed the typical undulating ‘wave’ appearance of axons in non-compressed nerve (asterisk array in H). However, these waves disappeared in the compressed nerve (see G), suggesting the compressed nerve was physically stretched during the compression. Notice that the intensity of axonal YFP was much weaker in the compressed nerves. This change has been very helpful for precisely defining the region of compression (please see supplementary Figure 1 for details). Within the compressed region, there were small islands of axons with strong intensity (arrows in 3G and supplementary Figure 1A) which likely were spared from compression forces. Insets: Caspr localization in paranodes was visualized under high power.

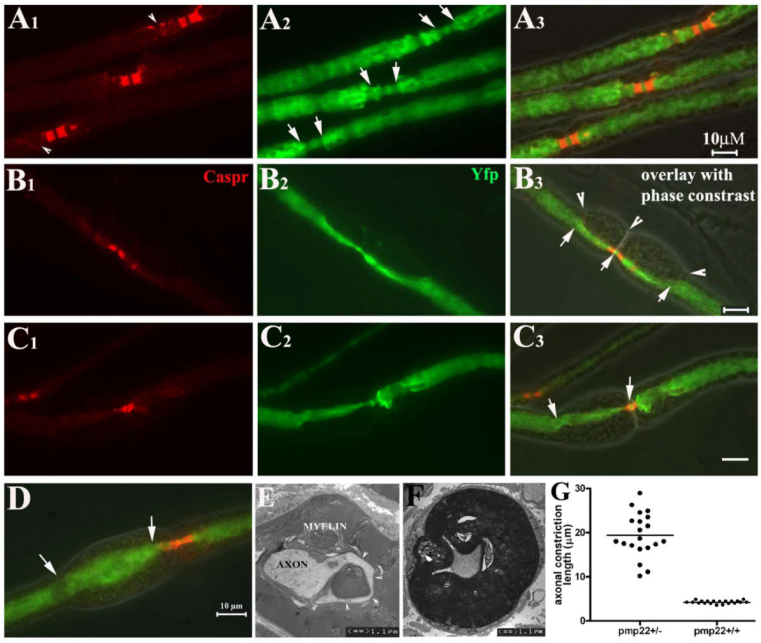

Figure 4.

Axonal constrictions in tomacula: All data in this figure were derived from non-compressed nerves. *Pmp22*+/− mice were cross-bred with *YFPtg*+/+ mice, so than all axons were labeled by YFP expressed from the *YFP* transgene. Sciatic nerves were dissected, fixed and teased into individual fibers, which were then stained with antibodies against Caspr. A1-3. Three nodes from 3 myelinated nerve fibers were flanked by the Caspr-stained paranodes. Some Caspr-spirals were also visible (arrowheads in A1). In the nodal/paranodal regions, there was a natural decrease of axonal diameter (between arrows in A2). There were no tomacula in these regions under phase-contrast imaging (overlay in A3). B1-3: Another myelinated nerve fiber was examined and showed tomacula in both paranodes that flanked the node of Ranvier (arrowheads in B3). Axonal segments in the tomacula were constricted and the narrowed axonal segments extended far beyond the paranodal regions (between arrows in B3). C1-3: A *pmp22*+/− myelinated nerve fiber had an asymmetry in its paranodes. The left paranode was affected by a tomaculae with constricted axon (between arrows in C3). In contrast, the right paranode with no tomaculae showed a normal axonal diameter. D. In some tomacula, axons may become enlarged (between arrows in D). E. The appearance of the enlarged axon in D is consistent with the EM finding in E. Axonal membranes occasionally became convoluted along the folding of myelin in tomaculae (arrowhead array). This membrane would appear enlarged when it is labeled by YFP and viewed under light microscopy. F. A constricted axon on transverse section. G. The length of normal paranodal axons and constricted axonal segments was measured in randomly selected fibers (diameters of these selected fibers were comparable between the groups), and showed in this histogram (4.2±0.2 μm for normal paranodal axons v.s. 19.4±4.9 μm for constricted axonal segments; $p<0.0001$).

Table 1

Primary antibodies

Antibody	Source	Species raised in	Specific antigen	Type	Reference
MAG	Zymed Laboratories # 34-6200	Rabbit	The shared C-terminal region of the small and large MAG	Polyclonal	Gotow et al. 1994
Kv1.2	Sigma # P 8732	Rabbit	GST fusion protein with aa417-498	Polyclonal	Mckinnon, et al 1989
Pan-Na_v	Sigma # S 8809	Mouse	Synthetic peptide CTEEQKKYYNAMKKLGSKK	Polyclonal IgG	Ulzheimer et al.,2004
Caspr	Dr. Pelles	Rabbit	Rat cytoplasmic domain	Polyclonal IgG	Einheber et al.,1997
MBP	Chemicon #MAB 386	Rat	aa82-87 , Bovine MBP	Monoclonal IgG	Li et al., 2005

Table 2

Recovery of CB in *pmp22*+/− mice

Genotype	No Recovery		Recovery	
	3 days	5 days	3 days	5 days
WT	2[a]/5[b] (40%)	1/7 (14%)	3[c]/5[d] (0[e]p)	6/7(1p)
PMP22+/−	4/4 (100%)	4/7 (57%)	0/4 (0p)	3/7(2p)

[a] = animals with no recovery;

[b] = total animals in this group;

[c] = animals with recovery;

[d] = total animals in this group;

[e] = animals with partial recovery; p = partial recovery.

Table 3

Prevalence of tomacula and axonal constrictions in *pmp22*+/− mice

Age	Tomacula (%)	Axonal Constrictions (%)	Axonal Enlargement (%)
3 months (n=6 mice)	45.3±0.4%[1]	26.7±7.5[2] or 12.1±3.4[1]	5.3±3.7[2]
6 months (n=5 mice)	48.4±12.3%[1]	32.0±9.9[2] or 15.9±4.8[1]	4.0±2.5[2]

[1] = % of all counted myelinated nerve fibers;

[2] = % of myelinated fibers with tomacula